Model Order Reduction of Bearingless Reluctance Motor Including Eccentricity

Model Order Reduction of Bearingless Reluctance Motor Including Eccentricity

Mehrnaz Farzam Far, Victor Mukherjee, Floran Martin, Paavo Rasilo, Anouar Belahcen, *Senior member, IEEE*

***Abstract* -- Eccentricity in a bearingless motor may occur during different operating states of the machine. This rises challenges in designing robust control for the machine with a lumped parameter model, due to the cross coupling of the windings with respect to the eccentric position of the rotor, the saturation of the ferromagnetic material, and spatial complexity. The non-linearity of the ferromagnetic material and the spatial harmonics can be considered in a finite element model of the machine, although applying it in a real time system is unreasonable. We propose a novel method based on orthogonal interpolation to reduce the order of the 2D finite element model of a bearingless synchronous reluctance motor, suitable for implementation in a real-time system. The winding currents and the eccentricity are given as inputs to the reduced model and the nodal values of the magnetic vector potential is obtained as the output, wherefrom the flux linkages, torque, and forces can be computed easily.**

***Index Terms*--Bearingless synchronous reluctance motor, eccentricity, finite element analysis, model order reduction, orthogonal interpolation method.**

I. INTRODUCTION

BEARING failure is one of the major problems in electrical machines during their operational lifetime. The bearing failures exaggerate further, when the machines operate at high speed or in abrasive conditions where the bearings suffer from contamination from the surrounding. Active magnetic bearings (AMBs) are considered as an alternative solution to avoid the mechanical bearing failures, especially in the high speed drives. However, using the AMBs in both sides of the shaft increases the overall length of the shaft, which in turn increases the flexural vibrations of the shaft in the high speed operation [1]. Therefore, applying the AMBs has certain limitation from the perspectives of rotor dynamics, cost effectiveness, and compactness. The bearingless motors have been proven as an alternative feasible solution to the mechanical bearings [2].

The bearingless motors can be considered as an integration of the functionality of the AMBs in a traditional motor. Two sets of windings are typically placed in the slots to create a flux imbalance over the airgap under different poles, which leads to the generation of electromagnetic forces. One common way to do this is having an additional winding with a one pole-pair difference with respect to the main motor winding [3]. In this paper, the bearingless motor under investigation has a traditional 2-pole-pair distributed winding as the main winding for generating the torque, and a 1-pole-pair distributed winding as an additional winding, to interact with the main winding and generate the electromagnetic forces.

To produce the necessary torque and the electromagnetic forces, the bearingless motor needs an active control of the current in both windings. The electromagnetic forces are controlled in a way that they oppose the gravitational forces of the rotor and the shaft, thus providing the necessary levitation for the rotating system. The bearingless motors can be classified similarly as the traditional motors. Each topology of bearingless motor has its own complexity of operation. In this paper, a synchronous reluctance motor (SynRM) is investigated for the bearingless operation [4].

The SynRM is devoid of any rotor bar or permanent magnet, which makes it cheaper and more robust, with less eddy current losses in the rotor, in comparison with the induction motor and the permanent magnet motor. The torque in a SynRM is generated by the differences of the reluctances in the rotor due to the position of the flux barriers [5]. The operation of a bearingless synchronous reluctance motor (BSynRM) is also influenced by the saliency as presented in [6], [7]. Moreover, the bearingless motor during its idle operation rests on the safety bearing, which incurs a static eccentricity during its startup. Nevertheless, during its normal operation with levitation, the rotor is subjected to different eccentricity due to the lack of ideal control and absence of any mechanical bearing. Therefore, to calculate the flux linkages in the different windings for the control of the motor, the information of the displacements of the rotor are taken into account along with the current vectors of the main winding and the additional winding. 1-D lumped parameter models as presented in [6], [7] can model this multi-input complexity, but it suffers from inaccuracy especially due to the saturation appearing from the non-linearity of the ferromagnetic material, as well as the complexity of the rotor design. The coupling between the main winding and additional winding especially in the non-linear region of the ferromagnetic material is very complex to model. There is a lack of good models in the existing literature, which can address this multi-input complexity for the bearingless operation.

The finite element (FE) models take into account the spatial harmonics and the non-linearity of the ferromagnetic material successfully. The FE analysis of BSynRM is already

This work was supported by the Academy of Finland, Helsinki, Finland, under Grant 287395 and Grant 297345 and the Estonian Research Council under grant PUT1260.

M. Farzam Far, V. Mukherjee, F. Martin, and A. Belahcen are with the Department of Electrical Engineering and Automation, Aalto University, Finland, 00076 Aalto, Finland (e-mail: firstname.lastname@aalto.fi).

A. Belahcen is also with Department of Electrical Power Engineering and Mechatronics, Tallinn University of Technology, 19086 Tallinn, Estonia.

P. Rasilo, is with the Laboratory of Electrical Energy Engineering, Tampere University of Technology, FI-33010 Tampere, Finland (e-mail: paavo.rasilo@tut.fi).

presented in [4]. However, applying the FE model in a real-time system is challenging due to the demanding computational resources.

Model order reduction (MOR) methods are commonly applied to reduce the complexity of a large-scale system by maintaining the input-output characteristic of the system in full measure. Although MOR is considerably a new concept in the field of electrical machines, several researchers [8]-[11] have demonstrated the efficiency of various methods of MOR on the order reduction of electrical machines. In [12], the BSynRM modelled with the proper orthogonal decomposition (POD) method has shown promising results especially in modelling the spatial complexity. In real-time application, however, the reduced model needs to avoid the iterative methods, such as the Newton-Raphson iteration scheme, to facilitate the process of computing. An alternative solution for this is presented in [13], where the reduced model of a traditional permanent magnet motor is built by using orthogonal interpolation method (OIM). Here, the terminal current of the permanent magnet motor is the only input parameter of the reduced model. Reference [13] also demonstrates the high efficiency of OIM in comparison with the nonlinear FE machine model and the corresponding reduced model based on POD coupled with discrete empirical interpolation method (POD-DEIM).

In this paper, we propose a novel OIM model for a 2D FE model of a bearingless motor with six input parameters, i.e. two components of the current vector of the main winding, two components of the current vector of the additional winding, and two displacement components of the rotor in the x-y plane. The OIM model performs 6-dimensional interpolation to estimate the nodal values of the vector potential at any given current excitations and rotor eccentricity. To the best knowledge of the authors, there is no reduced order model that considers the rotor eccentricity in the existing literature. The presented OIM model can be further used to compute easily the flux linkages in the windings, the electromagnetic forces on the rotor, and the torque of the BSynRM by post-processing of the OIM output data. This model can be applied as a novel way to control a bearingless motor in general in real-time.

II. NUMERICAL MODEL

A. System of equations

The single-component magnetic vector potential is often used to solve 2D magnetic problems. The governing equation of a static electromagnetic field problem, obtained from Maxwell's equation, is:

$$\nabla \times (\nu \nabla \times \boldsymbol{A}) = \boldsymbol{J} \tag{1}$$

where ν is the magnetic reluctivity of the material, $\boldsymbol{A}$ the magnetic vector potential, and $\boldsymbol{J}$ the current density in the coils of the machine.

The implementation of the FE method to the field problem leads to the algebraic system of equations:

$$\boldsymbol{S}\boldsymbol{a} = \boldsymbol{f} \tag{2}$$

where $\boldsymbol{S}$ is the stiffness matrix with size of $n \times n$. n is the number of degrees of the freedom (DoF) of the system of the equations, which is the same as the number of nodes in the FE mesh. $\boldsymbol{a} = [a_1 \dots a_n]^{\mathrm{T}}$ is the vector of the nodal values of the vector potential, and $\boldsymbol{f}$ the $n \times 1$ source vector originated from the current density.

In nonlinear materials, the stiffness matrix depends on the nodal values of the vector potential and thus (2) is nonlinear. In this case, a Newton-Raphson iteration scheme is commonly employed to solve the system of equations for $\boldsymbol{a}$.

One can calculate the three phase flux linkages of the stator coils, by the knowledge of the corresponding magnetic vector potential:

$$\psi = \frac{Nl}{C_{\mathrm{T}}} \int_{\Omega} \xi \boldsymbol{A} \mathrm{d}\Omega \,, \tag{3}$$

where N is the number of turns in the windings, l the axial length, and C_{T} the total cross-sectional area of one coil side of the winding. The integration is performed along the coil. Depending on the orientation of the coil side, ξ is defined as 1 or -1. The flux linkage in d- and q-axes can be computed using Park's transformation. Furthermore, the torque and the forces are also obtained based on the Coulomb's method [14].

B. Orthogonal decomposition method

The aim of the OIM is to represent the system of equations in terms of orthogonal functions, where the system input parameters (voltage, current, rotation angle, eccentricity, etc.) are the variables of the functions. This method of presenting the system reduces the order of the system, complexity, and consequently the computational cost. Like some other reduced models, the OIM consists of applying the singular value decomposition (SVD) on a set of precomputed data. The set of data is a set of samples, collected from the system at different operating points and stored in a matrix known as a snapshot matrix. However, unlike other methods, the OIM is constructed based on the right-singular vectors of the snapshot matrix.

Let us assume that $\boldsymbol{A}_{\mathrm{s}}$ is the snapshot matrix with size of $n \times m$, where n and m are the number of DoFs and the number of samples, respectively. One can compute the left-singular vectors (columns of $\boldsymbol{U}$), the singular values (diagonal entries of $\boldsymbol{\Sigma}$), and the right-singular vectors (columns of $\boldsymbol{V}$) of $\boldsymbol{A}_{\mathrm{s}}$ by SVD as $\boldsymbol{A}_{\mathrm{s}} = \boldsymbol{U}\boldsymbol{\Sigma}\boldsymbol{V}^{\mathrm{T}}$. Assuming the snapshot matrix represents the system correctly, the product $\boldsymbol{U}\boldsymbol{\Sigma}$ remains constant for any arbitrary values of input selected within the range of the snapshot matrix [13]. Hence, the prediction of the system output depends only on the right-singular vectors in $\boldsymbol{V}$; each column of $\boldsymbol{V}^{\mathrm{T}}$ corresponds to a specific operating point g within the snapshot matrix as:

$$\boldsymbol{A}_{\mathrm{s}} = \begin{pmatrix} a_{11} & \cdots & a_{1m} \\ \vdots & \ddots & \vdots \\ a_{n1} & \cdots & a_{nm} \\ \uparrow & & \uparrow \\ g_1 & \cdots & g_m \end{pmatrix} \xrightarrow{\mathrm{SVD}} \boldsymbol{V}^{\mathrm{T}} = \begin{pmatrix} v_{11} & \cdots & v_{1m} \\ \vdots & \ddots & \vdots \\ v_{m1} & \cdots & v_{mm} \\ \uparrow & & \uparrow \\ g_1 & \cdots & g_m \end{pmatrix}. \tag{4}$$

In this orthogonal basis, any new input set can be expressed as a vector sum of orthogonal vectors. The components of this new vector ($\hat{v}_1$, $\hat{v}_2$…, $\hat{v}_m$) can be independently interpolated with the corresponding

components of the right-singular vectors as functions of the original input quantities (voltage, current, rotor angle, eccentricity, etc.):

$$\hat{\boldsymbol{V}}_{\text{new}} = \begin{pmatrix} \hat{v}_1 \\ \hat{v}_2 \\ \vdots \\ \hat{v}_m \end{pmatrix}^{\text{T}} = \begin{pmatrix} f_1(\boldsymbol{x}_1, \boldsymbol{x}_2, \ldots \boldsymbol{x}_m) \\ f_2(\boldsymbol{x}_1, \boldsymbol{x}_2, \ldots \boldsymbol{x}_m) \\ \vdots \\ f_m(\boldsymbol{x}_1, \boldsymbol{x}_2, \ldots \boldsymbol{x}_m) \end{pmatrix}^{\text{T}}. \quad (5)$$

Generally, the functions can be multi-dimensional polynomials or Fourier series, etc [13]. The nodal values of the magnetic vector potential for this new input set is obtained as:

$$\boldsymbol{a}_{\text{new}} = \boldsymbol{U}\boldsymbol{\Sigma}\hat{\boldsymbol{V}}^{\text{T}}_{\text{new}}. \quad (6)$$

If the number of snapshots is less than the DoF ($m << n$), the OIM reduces the size of the problem and the computational complexity of (2) significantly. An additional reduction is obtained due to the SVD properties; the first r ($r << m << n$) singular values have the highest energy of the system and the remaining singular values have values very close to zero [15]. Thus, the order of the problem drops to r by selecting only r columns of $\boldsymbol{V}$ that correspond to the first r singular values.

III. Application to BSynRM

A. Topology

The OIM method is applied to a BSynRM FE model to study the eccentricity effects on the produced flux linkages of the machine. The motor parameters are presented in Table I.

TABLE I
PARAMETERS OF THE SYNCHRONOUS RELUCTANCE MACHINE

Parameter	Value Unite
Power	4,5 kW
Voltage	180 V
Current	16 A
Power factor	0,56
Frequency	50 Hz
Connection	Star
Number of pole pairs, main winding	2
Number of pole pairs, additional winding	1
Stator outer diameter	235 mm
Stator inner diameter	145 mm
Air gap	1 mm
Number of slots	36
Parallel branches	1

An in-house finite element software FCSMEK has been used for the numerical computations. The mesh and the flux density of the motor at rated load and levitation operation are presented in Fig. 1. First order mesh elements are used for the FE computations. The generated number of elements and nodes are 7480 and 4375, respectively.

The windings are supplied in a way that the 4-pole flux and the 2-pole flux are acting in the same direction in the positive y-axis and opposing each other in negative y-axis as shown in Fig. 1. Consequently, the Maxwell stress tensor is higher in the positive y-direction and generating the electromagnetic forces in the positive y-direction. Controlling this force will provide the necessary levitation force for the rotor and the shaft. It can be also seen from Fig. 1 that there is certain unequal distribution of flux density along the x-axis. This unequal distribution cases a force known as the disturbance force in a bearingless motor operation. The goal of the control system is to control the additional winding current in such a way that the disturbance force is always minimum, and the levitation force is always maximum for a given current amplitude.

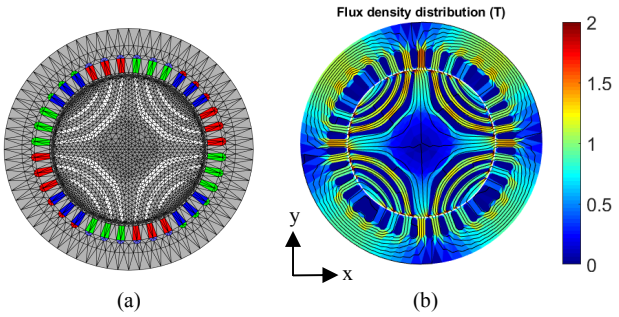

Fig. 1. (a) The first order mesh of the prototype with two windings, the additional winding can be seen in the bottom of the slots, (b) the magnetic flux density of the motor during the rated load and levitation force production state. Unequal flux density distribution between upper and lower parts of the airgap can be noticed.

B. Modeling eccentricity

When the rotor center is displaced from the stator center point, there is an unequal distribution of the airgap as shown in Fig. 2. If the unequal distribution of airgap remains fixed with respect to the rotation of the rotor, the effect is known as static eccentricity [16]. In this paper, we focus on stationary computation of the motor, so only the static eccentricity has been modelled to understand the system.

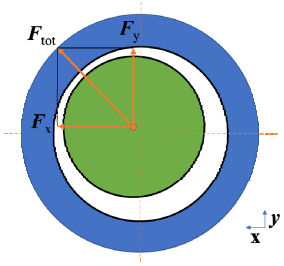

Fig. 2. The rotor center is displaced x units in the negative x-axis and y units in positive y-axis from the stator center, as a result the electromagnetic force has been produced towards the shortest airgap.

Now it is worth to remember that the eccentricity harmonics have also the ±1 pole pair difference with respect to the supplied winding. This means that the eccentric harmonic caused by the main winding has also a 1-pole pair flux density harmonic [16]. Therefore, the flux density distribution is widely affected by the eccentricity and thus its impact on the levitation force production is quite significant. Fig. 3 presents the flux density of the motor at two different

eccentric conditions.

It can be clearly seen from Fig. 3 that even at the rated current in the main and additional windings, the flux density distribution has changed from what is presented in Fig. 1. In Fig. 3(a), the rotor is displaced by 0.7 mm towards the positive x direction from the stator center. In this case, the dominant electromagnetic force is in x direction, which generates big disturbance forces. Therefore, to control the rotor at constant levitation, the understanding of the mutual coupling of the windings with the eccentricity is essential. In Fig. 3(b), the rotor is displaced towards the negative y direction from the stator center. This condition is quite common when the rotor rests on the safety bearing as mentioned before. Here, despite having rated additional winding current, the maximum force is produced in the negative y direction. Indeed, to produce the levitating electromagnetic force, much higher current than the rated current is needed in the additional winding.

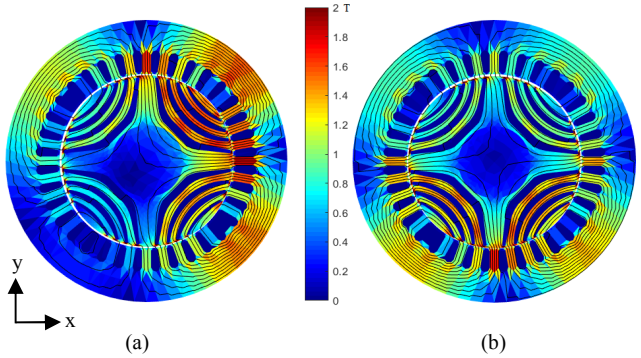

Fig. 3. Magnetic flux density distribution of the motor at rated current in main and additional winding when the rotor is (a) eccentric in positive x-direction, (b) eccentric in negative y-direction.

C. OIM model based on six input parameters

In this paper, we apply an OIM model based on 6 input parameters to reduce the order of the BSynRM model. The snapshot matrix, built for the order reduction, has the following input parameters:

a. 3 values for the spaced displacement of the rotor from the stator center in x-axis of the motor: d_x = [-0.2, 0, 0.2] mm.
b. 3 values for the spaced displacement of the rotor from the stator center in y-axis of the motor: d_y = [-0.2, 0, 0.2] mm.
c. 5 values for the d components of the main winding: i_{md} = [0, 5, 10, 15, 20].
d. 3 values for the q components of the main winding: i_{mq} = [0, 5, 10].
e. 3 values for the d components of the additional winding: i_{sd} = [-2, 0, 2].
f. 3 values for the q components of the additional winding: i_{sq} = [-2, 0, 2].

These parameters are selected in such a way that the snapshot matrix covers the nonlinear operating region and therefore the material non-linearity is considered in the OIM model as well. It is also worth mentioning that in this paper, we build the reduced model in the rotor reference frame and therefore the parameters are presented in the d-q coordinate system. One can indeed construct the reduced model in the stator reference frame by transferring the parameters to the stator reference frame and adding the angle of the rotor as the seventh parameter.

After solving the FE model of the motor with all the possible combinations of the input parameters ($3^2 \times 5 \times 3^3$ = 1215), the solutions are stored in the snapshot matrix $\boldsymbol{A}_s$ with size of 4375 × 1215 in the following format, and thereafter $\boldsymbol{V}^T$ is calculated via SVD:

$$\begin{matrix} d_{x1}, d_{y1}, & \cdots & d_{x2}, d_{y1}, & \cdots & d_{x3}, d_{y3} \\ i_{md1}, i_{mq1}, & \cdots & i_{md1}, i_{mq1}, & \cdots & i_{md5}, i_{mq5} \\ i_{sd1}, i_{sq1} & \cdots & i_{sd1}, i_{sq1} & \cdots & i_{sd3}, i_{sq3} \\ \downarrow & & \downarrow & & \downarrow \end{matrix}$$

$$\boldsymbol{A}_s = \begin{pmatrix} a_{1,1} & \cdots & a_{1,406} & \cdots & a_{1,2025} \\ \vdots & \ddots & \vdots & \ddots & \vdots \\ a_{n,1} & \cdots & a_{n,406} & \cdots & a_{n,2025} \end{pmatrix}_{4375\times1215}, \qquad (7)$$

$$\boldsymbol{V}^T = \begin{pmatrix} a_{1,1} & \cdots & a_{1,406} & \cdots & a_{1,2025} \\ \vdots & \ddots & \vdots & \ddots & \vdots \\ a_{m,1} & \cdots & a_{m,406} & \cdots & a_{m,2025} \end{pmatrix}_{2025\times1215}.$$

The snapshot matrix has 1215 right-singular vectors, which means that we require 1215 functions to define the system of equations. Nevertheless, the first 17 singular values capture about 98 % energy of the system [9]. Therefore, the first 17 right-singular vectors are sufficient to describe the system of equations, i.e. the order of (2) drops from 4375 to 17 (r = 17). To obtain the functions from the right-singular vectors, a piecewise linear interpolation is performed on each column of $\boldsymbol{V}$.

D. Results

The accuracy of the proposed reduced model is evaluated in terms of the nodal values of the magnetic vector potential. The FE model and the reduced model are solved for 100 different operating points. These operating points are randomly selected from the interval of the input parameters, within the snapshot range. Fig. 4 presents the percentage of the relative errors for these 100 operating points.

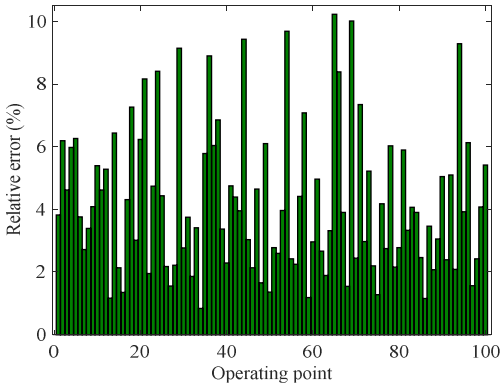

Fig. 4. Percentage of relative error between the nodal vales of the magnetic vector potentials obtained by FE method and OIM at different operating points.

Depending on the operating point, the relative error changes from 0.8 % to 10 %. The relative error for an operating point in percentage is defined as:

$$\varepsilon = \frac{\left\| \boldsymbol{a}_{\mathrm{FEM}} - \boldsymbol{a}_{\mathrm{OIM}} \right\|}{\left\| \boldsymbol{a}_{\mathrm{FEM}} \right\|}. \tag{8}$$

where $\boldsymbol{a}_{\mathrm{FEM}}$ and $\boldsymbol{a}_{\mathrm{OIM}}$ are of the nodal values of the magnetic vector potentials obtained from FE method and OIM, respectively.

Furthermore, the consistency and accuracy of the OIM model is examined by varying one input parameter and keeping the other five input parameters constant. In the first case, the five constant parameters are: i_{md} = 15 A, i_{mq} = 7 A, i_{sd} = 2 A, i_{sq} = 0 A, d_{y} = 0.18 mm; and d_{x} varies from -0.2 mm to 0.2 mm. The flux linkage components of the main and the additional windings, computed from FE model, are presented in Fig. 5(a). Fig. 5(b) shows the relative error percentage between these flux linkages and the ones resulting from the OIM.

In the second case, d_{y} varies from -0.2 mm to 0.2 mm, d_{x} = 0.18 mm, and the rest of the parameters are kept the same as in the first case. The results of this case are shown in Fig. 6. The FE flux linkages match well with the results of OIM. Moreover, the relative errors can be reduced to zero by coupling the OIM method with the DEIM or applying Newton-Raphson iteration on the OIM results. However, we want to avoid the iterative methods to build a more efficient model in terms of computation time, which can be employed in the real-time system.

In addition, we compare the levitation force of the BSynRM as presented in Fig. 7, which is the electromagnetic force in the y-direction in this geometry. Fig. 7(a) shows the FE model levitation force varying as a function of the rotor displacement along the x- and y- axes from -0.1 mm to 0.1 mm. Fig. 7(b) shows the relative error percentage of the levitation force at each point calculated from FE method and OIM method. The current components are kept same as in the previous cases. The highest error, about 3 %, occurs at d_{x} and d_{y} equal to -0.1 mm.

In terms of computational time, the OIM reduces the computational time significantly. The average computational time of FE method is about 600 ms. The computational time drops to 0.4 ms by using the OIM. This time does not include the required time for computing the snapshot matrix or the construction of the reduced model. However, it should be noted that the process of making the snapshot matrix and building the reduced model is performed in advance; once the

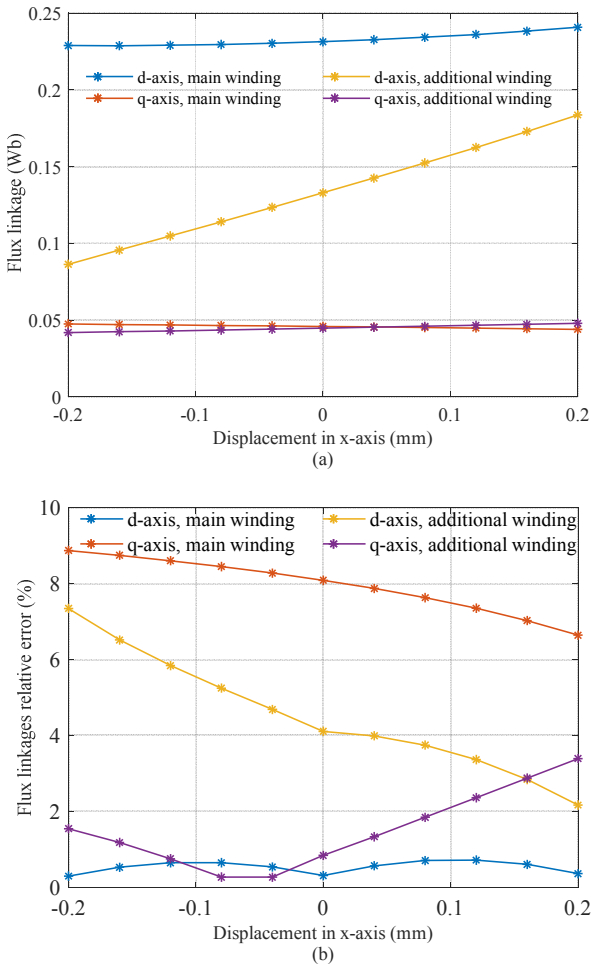

Fig. 5. (a) Flux linkage components, obtained by FE method with respect to the rotor displacement in x-axis; (b) relative error percentage of flux linkages in main and additional windings, calculated from FE method and OIM.

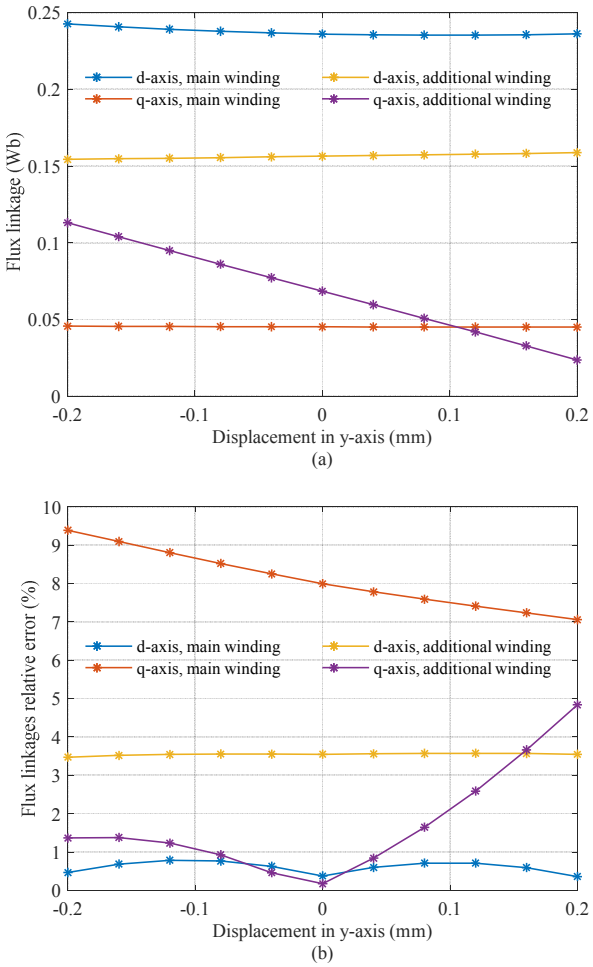

Fig. 6. (a) Flux linkage components, obtained by FE method with respect to the rotor displacement in y-axis; (b) relative error percentage of flux linkages in main and additional windings, calculated from FE method and OIM.

reduced model is built, it is an efficient substitute for the FE model, especially in applications such as real-time control in which efficiency in the computational time is crucial.

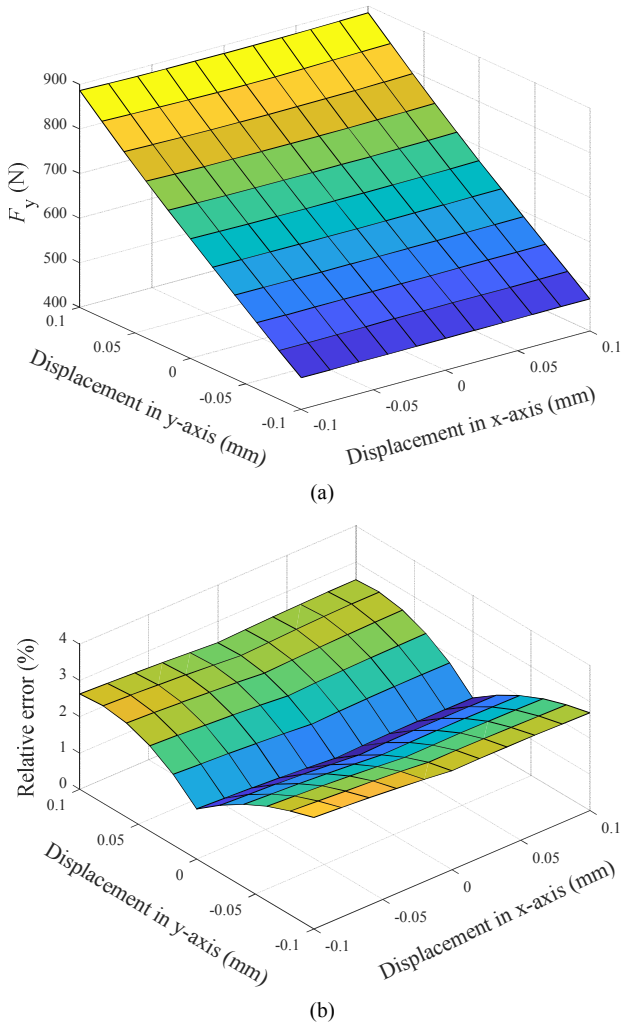

Fig. 7. (a) The electromagnetic force in y direction computed as a function of the displacement of the rotor in x- and y-axes using FE method, (b) the relative error percentage of forces, calculated from FE method and OIM method.

IV. Conclusion

In this paper, we present a novel OIM model of a bearingless motor with six input parameters. These input parameters are the d- and q-axis currents of the main winding, the d- and q-axis currents of the additional winding, and the x- and y-axis displacements of the rotor. The OIM model performs a piecewise linear interpolation to estimate the vector potential at any given current excitations and rotor eccentricity. The flux linkages in the windings and the electromagnetic forces on the rotor are computed by post-processing of the OIM output data.

We examine the proposed method on a BSynRM, however, the method can be used for any other synchronous machine in which the effect of eddy current is negligible. For validation purposes, we compare the OIM model with the FE model, in terms of the vector potential, the flux linkages, the produced electromagnetic forces of the motor, and the computational time. The OIM significantly reduces the computational time, and the flux linkages and the electromagnetic forces obtained from the OIM model match the FE model results with minor variations. These minor variations, however, are constant within the snapshot interval and we will address these variations by introducing a suitable coefficient in the future work. Assuming the FE model presents the bearingless motor accurately, the corresponding reduced model will be suitable for implementing in the real-time control of the motor.

V. References

[1] S. Zheng, H. Li, C. Peng, and Y. Wang, "Experimental investigations of resonance vibration control for noncollocated AMB flexible rotor systems," *IEEE Trans. Ind. Electronics*, vol. 64, no. 3, pp. 2226-2235, Mar. 2017.

[2] T. Reichert, T. Nussbaumer, and J. W. Kolar, "Bearingless 300 W pmsm for bioreactor mixing," *IEEE Trans. Ind. Electronics*, vol. 59, no. 3, pp. 1376-1388, Mar. 2012.

[3] A. Chiba, "Magnetic bearings and bearingless drives," Amsterdam: Elsevier/Newnes, 2005.

[4] A. Belahcen, V. Mukherjee, M. F. Far, P. Rasilo, and M. Hinkkanen, "Coupled field and space-vector equations of bearingless synchronous reluctance machine," *2016 XXII Int. Conf. Electrical Machines (ICEM)*, Lausanne, 2016, pp. 2581-2587.

[5] G. Pellegrino, P. Guglielmi, A. Vagati, and F. Villata, "Core losses and torque ripple in IPM machines: dedicated modeling and design tradeoff," *IEEE Trans. Ind. Applications*, vol. 46, no. 6, pp. 2381-2391, Nov.-Dec. 2010.

[6] A. Chiba, M. Rahman and T. Fukao, "Radial force in a bearingless reluctance motor," *IEEE Trans. Magnetics*, vol. 27, no. 2, pp. 786-791, Mar. 1991.

[7] S. E. Saarakkala, M. Sokolov, V. Mukherjee, J. Pippuri, K. Tammi, A. Belahcen, and M. Hinkkanen, "Flux-linkage model including cross-saturation for a bearingless synchronous reluctance motor," in Proc. ISMB15, Kitakyushu, Japan, Aug. 2016.

[8] L. Montier, T. Henneron, S. Clénet, and B. Goursaud, "Transient simulation of an electrical rotating machine achieved through model order reduction," *Advanced Modeling and Simulation in Engineering Sciences*, vol. 3, no. 10, pp. 1-17, Mar. 2016. Available: https://doi.org/10.1186/s40323-016-0062-z

[9] M. Farzamfar, A. Belahcen, P. Rasilo, S. Clénet, and A. Pierquin, "Model Order Reduction of Electrical Machines With Multiple Inputs," *IEEE Trans. Ind. Applications*, vol. 53, no. 4, pp. 3355-3360, Mar. 2017.

[10] H. Ebrahimi, Y. Gao, and K. Muramatsu, "Fast Nonlinear Magnetic Field Analysis of Inverter-Driven Machines by Applying POD on Linearized Coefficient Matrices," *IEEE Trans. Magnetics*, vol. 53, no. 6, pp. 1-4, June 2017.

[11] L. Montier, T. Henneron, S. Clénet, and B. Goursaud, "Proper Generalized Decomposition Applied on a Rotating Electrical Machine," *IEEE Trans. Magnetics*, no. 99, pp. 1-4, Nov. 2017.

[12] V. Mukherjee, M. F. Far, F. Martin and A. Belahcen, "Constrained algorithm for the selection of uneven snapshots in model order reduction of a bearingless motor," in *IEEE Trans. Magnetics*, vol. 53, no. 6, pp. 1-4, June 2017.

[13] M. Farzam Far, F. Martin, A. Belahcen, L. Montier, and T. Henneron, "Orthogonal Interpolation Method for Order Reduction of a Synchronous Machine Model," in *IEEE Trans. Magnetics*, vol. 54, no. 2, pp. 1-6, Feb. 2018.

[14] J. L. Coulomb, "A methodology for the determination of global electromechanical quantities from a finite element analysis and its application to the evaluation of magnetic forces, torques and stiffness," *IEEE Trans. Magnetics*, vol. 19, no. 6, pp. 2514-2519, Nov 1983.

[15] V. Klema and A. Laub, "The singular value decomposition: Its computation and some applications," *IEEE Trans. Automatic Control*, vol. 25, no. 2, pp. 164-176, Apr 1980.

[16] A. Sinervo and A. Arkkio, "Eccentricity Related Forces in Two-Pole Induction Motor With Four-Pole Stator Damper Winding Analyzed Using Measured Rotor Orbits," *IEEE Trans. Magnetics*, vol. 49, no. 6, pp. 3029-3037, June 2013.

VI. BIOGRAPHIES

Mehrnaz Farzam Far received the M.Sc. (Tech.) degree in electrical engineering from Aalto University, Espoo, Finland, in 2014, where she is currently working toward the D.Sc. degree in electrical engineering. Her research interest includes the numerical modeling of electrical machines.

Victor Mukherjee received the B.Sc. (Tech.) degree in electrical engineering from National Institute of Technology, Durgapur, India, and the M.Sc. (Tech) degree in industrial electronics from Lappeenranta University of Technology, Lappeenranta, Finland, in 2009 and 2014, respectively. He is currently working toward the D.Sc. degree in Aalto University, Espoo, Finland.

Floran Martin received his D.Sc. degree from University of Nantes in 2013. He is currently working as a Post-doctoral researcher in Aalto University, department of Electrical Engineering and Automation. His research is oriented toward magneto-mechanical effects in steel sheets and optimization of electrical machines.

Paavo Rasilo received his M.Sc. (Tech.) and D.Sc. (Tech.) degrees from Helsinki University of Technology (currently Aalto University) and Aalto University, Espoo, Finland in 2008 and 2012, respectively. He is currently working as an Assistant Professor at the Laboratory of Electrical Energy Engineering, Tampere University of Technology, Tampere, Finland. His research interests deal with numerical modeling of electrical machines as well as power losses and magnetomechanical effects in soft magnetic materials.

Anouar Belahcen (M13-SM15) received the M.Sc. (Tech.) and Doctor (Tech.) degrees from Helsinki University of Technology, Finland, in 1998, and 2004, respectively. He is now Professor of electrical machines at Tallinn University of Technology, Estonia and Professor of Energy and Power at Aalto University, Finland. His research interest are numerical modeling of electrical machines, magnetic materials, coupled magneto-mechanical problems, magnetic forces, magnetostriction, and fault diagnostics.